Real-time condition assessment of railway tunnel deformation using an FBG-based monitoring system

Lu Zhou[*1,2], Chao Zhang[1,2,a], Yi-Qing Ni[1,2,b] and Chung-Yue Wang[3c]

[1]*Hong Kong Branch of Chinese National Rail Transit Electrification and Automation Engineering Technology Research Center, Hong Kong*
[2]*Department of Civil and Environmental Engineering, The Hong Kong Polytechnic University, Hung Hom, Kowloon, Hong Kong*
[3]*Department of Civil Engineering, National Central University, Taoyuan, Taiwan*

Abstract. A tunnel deformation monitoring system is developed with the use of fiber Bragg grating (FBG) sensing technique, aiming at providing continuous monitoring of railway tunnel deformation in the long term, and early warning for the rail service maintainers and authorities to avoid catastrophic consequences when significant deformation occurs. Specifically, a set of FBG bending gauges with the ability of angle measurement and temperature compensation is designed and manufactured for the purpose of online monitoring of tunnel deformation. An overall profile of lateral tunnel displacement along the longitudinal direction can be obtained by implementing an array of the FBG bending gauges interconnected by rigid rods, in conjunction with a proper algorithm. The devised system is verified in laboratory experiments with a test setup enabling to imitate various patterns of tunnel deformation before the implementation of this system in an in-service high-speed railway (HSR) tunnel.

Keywords: railway tunnel deformation; online monitoring; FBG bending gauge array; temperature compensation

1. Introduction

Deformation of infrastructure systems such as bridges, tunnels and dams related to safety and maintenance issues has long been a major concern to the investors and asset managers. Tunnels are critical components of transportation networks responsible for safe and sustainable operation of railways, subways and highways (Wright 2010). Yet tunnels have the potential to cause the most catastrophic damage of an entire route because they are likely to deform critically during natural disasters such as earthquakes or landslides, especially for railway tunnels. Hence, it is vital and essential to monitor the railway tunnel deformation in a continuous and long-term manner to guarantee the normal and safe operation of trains and to provide timely warning of large deformation, which is particularly important today for high-speed railway (HSR) tunnels where trivial planar or transverse displacements of rail tracks may increase the risk of unstable operation or even derailment and time is limited for early warning and decision making.

There has been a large amount of research on monitoring deformation of civil infrastructure using various techniques and devices, including tape extensometers (Bernardo-Sánchez and Arlandi-Rodríguez 2014), total stations (Kontogianni and Stiros 2003), photogrammetry (Scaioni *et al.* 2014), and 3D laser scanners (Kavvadas

2005). Among the above, the tape extensometer is the most accurate one for deformation measurement, and easy to use (Bernardo-Sánchez and Arlandi-Rodríguez 2014). However, it can only be used to measure the distance changes relative to a fixed point and must be manipulated manually, which makes it incapable of continuous and long-term monitoring of railway tunnel deformation.

Total station is commonly utilized in measuring tunnel deformation with its advantages of non-contact and relatively high accuracy (Kontogianni and Stiros 2003, Luo *et al.* 2016, Ordóñez *et al.* 2016). Tse and Luk (2011) developed an automatic deformation monitoring system (ADMS) using total stations, and applied this system to the deformation measurement of the Cross-Harbour Tunnel in Hong Kong. As this technique is vulnerable to environmental interferences, it is not applicable to online monitoring of railway tunnels where the devices can be fully blinded by passing trains.

The laser scanning technique provides a new way to monitor tunnel deformation in recent years, enabling to get deformation information of an entire tunnel in a very short time. Nevertheless, its low accuracy with an error level of around ±5 mm (Yoon *et al.* 2009, Pejić 2013) limits its application in railway tunnel monitoring.

The environment of tunnels is generally harsh with numerous dust and large temperature variances throughout the whole year. In terms of railway tunnels specifically, the electric interferences are severe during the operation hours and intense vibrations are caused by passing trains. Therefore, it is highly desirable to develop a new approach suitable for long-term railway tunnel deformation monitoring which overcomes the limitations of the conventional techniques mentioned above.

∗Corresponding author, Postdoctoral Fellow, Ph.D.
 E-mail: lu.lz.zhou@polyu.edu.hk
[a] Research Assistant
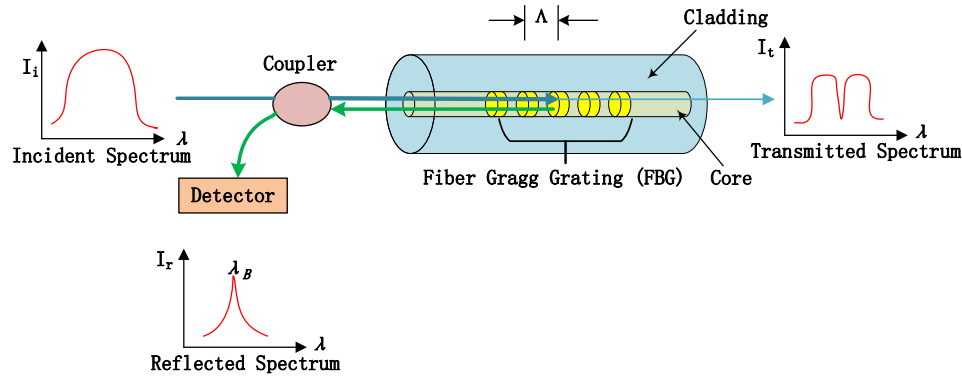[b] Professor and Director, Ph.D.
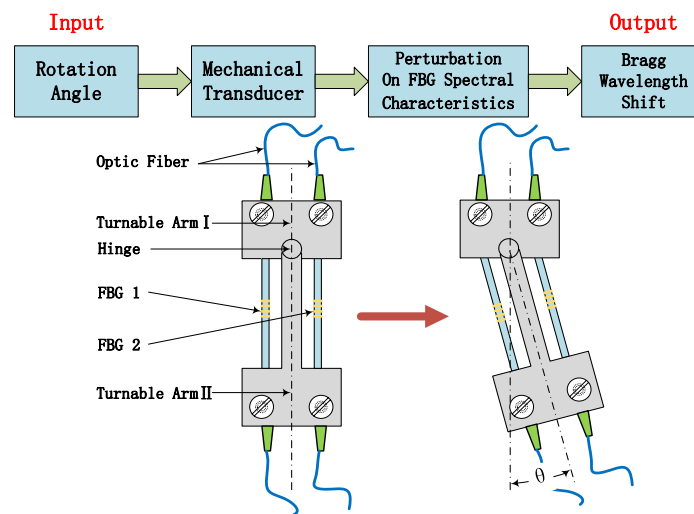[c] Professor, Ph.D.

Fig. 1 Principle of fiber Bragg grating

Fig. 2 Angle measurement using FBG bending gauge

Fiber Bragg grating (FBG), as a viable strain measuring technique, has been widely used for structural health monitoring (SHM) (Chan *et al.* 2006, Ni *et al.* 2009, Ye *et al.* 2014). FBG sensors have the advantages of small size, light weight, high accuracy, immunity to electromagnetic interference (EMI), and being adaptive to varying and harsh environments (Ye *et al.* 2013), making them suitable for railway tunnel deformation monitoring. Metje *et al.* (2008) developed a displacement monitoring system based on FBG 'Smart Rods' for measuring displacements of the tunnel lining with a series of 'bench test' conducted in laboratory.

A variety of inclinometers and deflectometers based on FBG have been developed and utilized for measuring deformation and settlement of geotechnical structures (Yoshida *et al.* 2002, Ding *et al.* 2013, Ye *et al.* 2013, Pei *et al.* 2014). Ho *et al.* (2006) presented a novel ground movement monitoring system based on FBG segmented deflectometer (FBG-SD) and conducted a series of indoor and field tests to estimate its performance. Zhu *et al.* (2012) developed a slope monitoring system which has been successfully applied for monitoring a roadside slope in Hong Kong.

In the present study, a novel online monitoring system is devised for monitoring lateral and vertical displacements of railway tunnels by deploying several chains of FBG bending gauges, which is able to reconstruct continuous deformation of railway tunnels and provide automatic condition assessment of in-service railway tunnels. FBG bending gauges with temperature self-compensation are designed and manufactured specifically to serve this purpose. Before its full-scale implementation to a HSR tunnel, the devised online monitoring system is verified through a series of laboratory experiments with various deformation patterns tested, subsequent to a test on the temperature compensation capability of the FBG bending gauges.

2. Development of FBG bending gauges and railway tunnel deformation monitoring system

2.1 Principle of FBG measuring technique

FBG is a type of distributed Bragg reflector embedded in a short segment of optic fiber which can reflect specific wavelengths of light by creating a periodic variation in the

refractive index of the fiber core. As shown in Fig. 1, a broadband light is emitted into the FBG and the specific wavelength (Bragg wavelength) is reflected with the rest parts transmitted through. The principle of FBG for strain and temperature measurement can be expressed through the following equations

$$\lambda_B = 2n_{eff}\Lambda \qquad (1)$$

$$\Delta\lambda_\varepsilon = (1 - p_e)\lambda_B\Delta\varepsilon \qquad (2)$$

$$\Delta\lambda_T = (\alpha + \xi)\lambda_B\Delta T \qquad (3)$$

$$\Delta\lambda_B = (1 - p_e)\lambda_B\Delta\varepsilon + (\alpha + \xi)\lambda_B\Delta T \qquad (4)$$

where λ_B is the Bragg wavelength, Λ is the period of the grating, and n_{eff} is the effective refractive index. The Bragg wavelength shift $\Delta\lambda_B$ comes in two parts: the wavelength shift $\Delta\lambda_\varepsilon$ caused by strain change, and the wavelength shift $\Delta\lambda_T$ caused by temperature variance. p_e is the photoelastic coefficient, α is the thermal expansion coefficient and ξ is the thermal optical coefficient.

Fig. 2 illustrates the design of an FBG bending gauge comprising two turnable arms and a revolution joint with one rotational degree of freedom which allows the two arms to rotate at an angel within $\pm 1°$. Two pre-tensioned FBGs are positioned on opposite sides with respect to the centerline of the turnable arm II to allow for the measurement of angle change. When subjected to bending, the sensor suffers from either tensile or compressive strains which will induce central wavelength shifts of the reflected light. The relative angle is measured, while the temperature effect is compensated as detailed in the following section.

2.2 Design of FBG bending gauge with temperature self-compensation

When a relative rotation between the turnable arm I and the turnable arm II occurs, the FBG on one side undergoes a tensile force while the FBG on the other side undergoes a compressive force. The corresponding central wavelength shifts of the two FBGs are $\Delta\lambda_1$ and $\Delta\lambda_2$, respectively. The wavelength shifts are induced by both strain and temperature variations, which can be expressed by

$$\Delta\lambda_1 = \lambda_{\varepsilon 1} + \lambda_{t1} \qquad (5)$$

$$\Delta\lambda_2 = \lambda_{\varepsilon 2} + \lambda_{t2} \qquad (6)$$

where $\lambda_{\varepsilon 1}$ and $\lambda_{\varepsilon 2}$ are the wavelength shifts caused by strains when rotation occurs, and λ_{t1} and λ_{t2} represent the wavelength shifts caused by temperature variation. The total central wavelength shift of the FBG bending gauge with a rotation angle θ is determined by

$$\Delta\lambda_\theta = \Delta\lambda_1 - \Delta\lambda_2 \qquad (7)$$

Since the two FBGs are spatially close to each other, the ambient temperature variation experienced by them can be assumed to be identical, that is, $\lambda_{t1} = \lambda_{t2}$. In this way, the influence of temperature is eliminated, and the measurement subtraction is fully resulting from strains

$$\Delta\lambda_\theta = \lambda_{\varepsilon 1} - \lambda_{\varepsilon 2} \qquad (8)$$

An experiment was carried out to verify the temperature compensation capability of the devised FBG bending gauge. As shown in Fig. 3, the sensor was placed in a temperature chamber, and an FBG interrogator was connected to the bending gauge and a laptop to collect and store central wavelength shift caused by temperature variation. Since the temperature inside the chamber cannot be guaranteed to be evenly distributed over the whole space, a pair of thermocouples were placed beside the two FBGs of the bending gauge to precisely capture the ambient temperature, and a data logger was used to record the temperature.
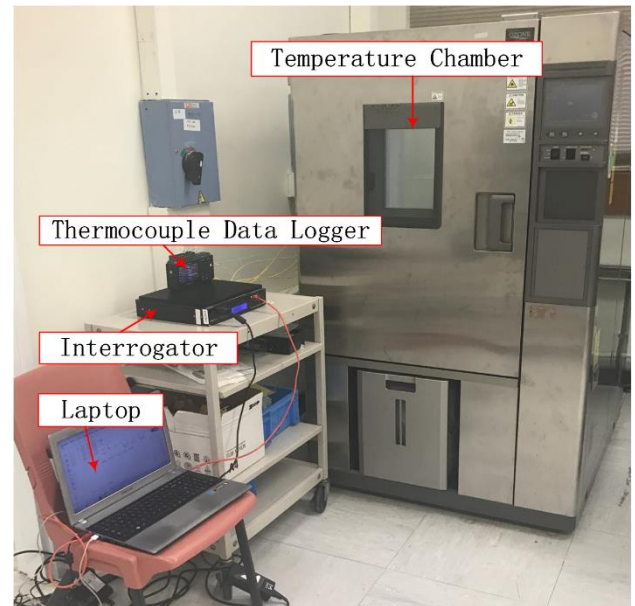

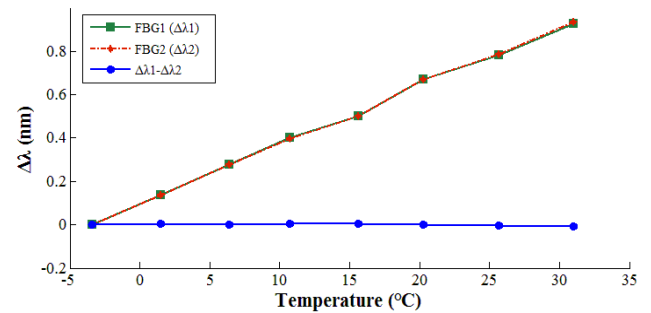Fig. 3 Experimental set-up for temperature compensation test

Fig. 4 Wavelength outputs of FBG bending gauge under different temperatures

The central wavelength shifts were measured separately for the two FBGs in the sensor, as plotted in Fig. 4, from which it is obviously seen that for all 8 temperature levels tested ranging from -4℃ to 31℃, the wavelength shifts measured from the two FBGs are almost identical, and their subtraction can be plotted as a straight zero-value line hardly affected by temperature fluctuations. It demonstrates that the FBG bending gauge has an excellent performance in compensating the effect due to temperature fluctuations.

2.3 Railway tunnel deformation monitoring using FBG bending gauges

When geological disasters such as landslides, earthquakes or ground settlements occur, the tunnel is likely to deform in both lateral and vertical directions and will distort at one or several cross-sections. Hence, one monitoring target of our study is to provide a comprehensive plot of lateral and vertical displacements as well as cross-sectional convergence. Fig. 5 shows the cross-sectional view when deploying 6 arrays of FBG bending gauges on a railway tunnel, which include the sensors installed on the tunnel side wall as well as on the rail slabs.

In the longitudinal view, the FBG bending gauges are implemented at nearly equal intervals along the longitudinal direction of the railway tunnel. These FBG bending gauges are interconnected by rigid rods to form a chain which stretches in alignment with the tunnel and deforms in an identical manner as the tunnel does, as shown in Fig. 6.
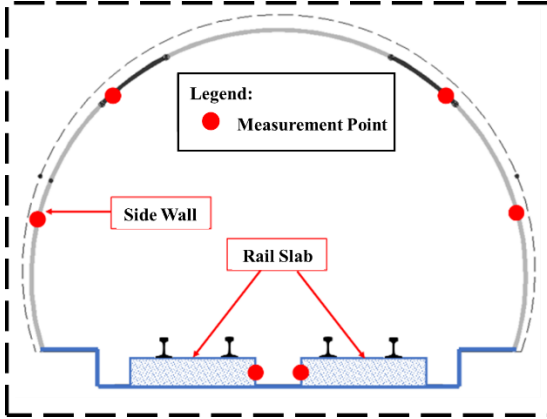

Fig. 5 Cross-sectional view of deployment of tunnel deformation monitoring system on railway
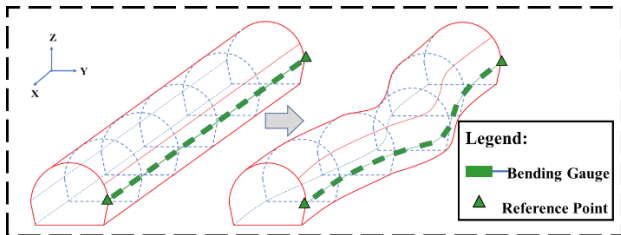

Fig. 6 longitudinal view of deployment of tunnel deformation monitoring system on railway

When deformation happens in the tunnel, the displacement of each FBG bending gauge can be calculated from the angles of rotation relative to its two adjacent bending gauges, as shown in Fig. 7. Eventually, a configuration of the chain after deformation can be derived with the aid of an appropriate algorithm to indicate the displacement profile of the tunnel.

Consider a chain formed with FBG bending gauges at distances denoted as $\{L_1, L_2, ..., L_{n-1}\}$. We can derive the absolute rotation angles $\{\theta_1, \theta_2, ..., \theta_n\}$ and the displacements $\{\delta_1, \delta_2, ..., \delta_n\}$ at the measuring points by using the measured relative rotation angles $\{\alpha_1, \alpha_2, ..., \alpha_n\}$. From the geometric relationship, the following equations can be written for the ith bending gauge

$$L_i \tan \theta_i = \delta_{i+1} - \delta_i \tag{9}$$

$$\alpha_i = \theta_i - \theta_{i-1} \tag{10}$$

Since the rotation angles would not be practically too large (between $-\pi/2$ and $\pi/2$), It is assumed here that the rotation angle is positive if it is counterclockwise and negative if it is clockwise for both α_i and θ_i. Eq. (9) is valid for $i = 1, ..., n-1$ while Eq. (10) is valid for $i = 2, ..., n$. With $\alpha_1 = \theta_1$, we can rewrite Eqs. (9) and (10) for all measuring points in matrix forms as follows

$$\begin{pmatrix} -1 & 1 & 0 & & 0 & 0 & 0 \\ 0 & -1 & 1 & \cdots & 0 & 0 & 0 \\ 0 & 0 & -1 & & 0 & 0 & 0 \\ \vdots & & & \ddots & & \vdots \\ 0 & 0 & 0 & \cdots & -1 & 1 & 0 \\ 0 & 0 & 0 & & 0 & -1 & 1 \end{pmatrix}_{(n-1)\times n}$$

$$\begin{pmatrix} \delta_1 \\ \delta_2 \\ \delta_3 \\ \vdots \\ \delta_{n-1} \\ \delta_n \end{pmatrix} = \begin{pmatrix} L_1 \tan \theta_1 \\ L_2 \tan \theta_2 \\ L_3 \tan \theta_3 \\ \vdots \\ L_{n-2} \tan \theta_{n-2} \\ L_{n-1} \tan \theta_{n-1} \end{pmatrix} \tag{11}$$

$$\begin{pmatrix} 1 & 0 & 0 & & 0 & 0 & 0 \\ -1 & 1 & 0 & \cdots & 0 & 0 & 0 \\ 0 & -1 & 1 & & 0 & 0 & 0 \\ \vdots & & & \ddots & & \vdots \\ 0 & 0 & 0 & & 1 & 0 & 0 \\ 0 & 0 & 0 & \cdots & -1 & 1 & 0 \\ 0 & 0 & 0 & & 0 & -1 & 1 \end{pmatrix}_{n\times n}$$

$$\begin{pmatrix} \theta_1 \\ \theta_2 \\ \theta_3 \\ \vdots \\ \theta_{n-1} \\ \theta_n \end{pmatrix} = \begin{pmatrix} \alpha_1 \\ \alpha_2 \\ \alpha_3 \\ \vdots \\ \alpha_{n-1} \\ \alpha_n \end{pmatrix} \tag{12}$$

The rank of the coefficient matrix in Eq. (11) is n-1, which is insufficient to get a deterministic solution. Therefore, the first FBG bending gauge is fixed with
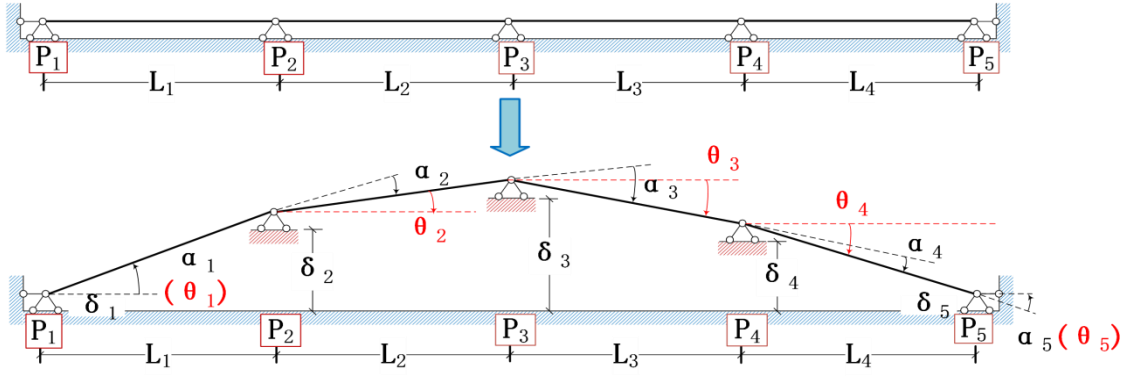
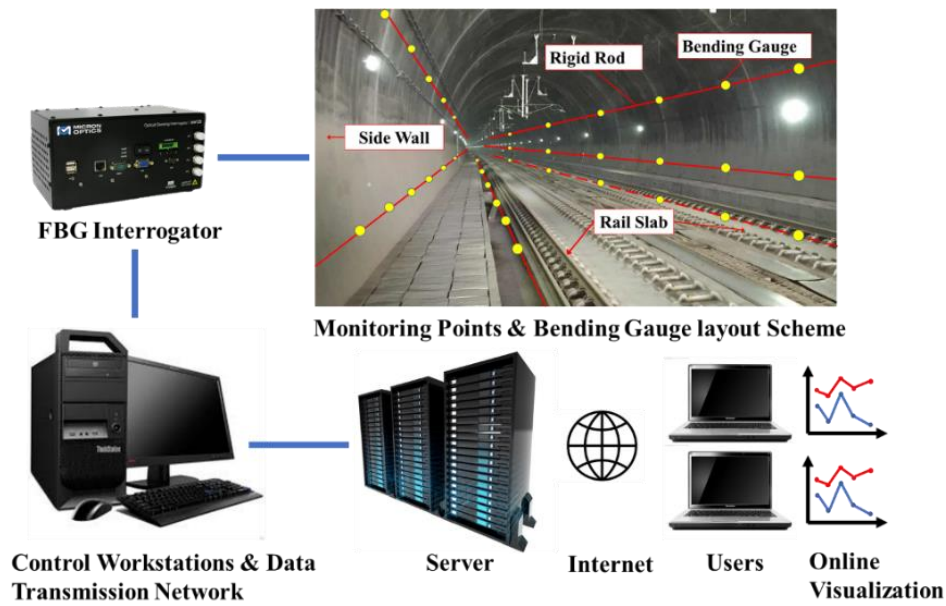Fig. 7 Displacement evaluation from measured rotation angles

Fig. 8 Topological structure of railway tunnel deformation monitoring system

$\delta_1 = 0$. As for Eq. (12), it can be easily seen that the coefficient matrix is full-rank, indicating there is a deterministic solution. In this way, the displacement profile can be derived from the measured relative rotation angles.

2.4 Hardware and software of railway tunnel deformation monitoring system

The devised railway tunnel deformation monitoring system has been implemented for real-time monitoring of an in-service HSR tunnel. As illustrated in Fig. 8, the system consists of four subsystems: 1) sensing system, 2) data acquisition system, 3) data storage, processing and analysis system, and 4) real-time display and visualization system.

The sensing and data acquisition subsystems include a number of FBG bending gauge arrays deployed at tunnel wall and rail slabs for online monitoring and continuous data acquisition, and an FBG interrogator that interprets the relative rotations between FBG bending gauges into central wavelength readings. As for the data storage, processing

and analysis subsystem, a workstation is used for data pre-processing such as de-noising, long-term trend extraction and advanced data analysis to plot time-variant deformation profiles in line with the FBG bending gauge arrays; and an online cloud database is used for storage of the collected and processed online monitoring data. The real-time display and visualization is realized by a front-end web accessible to authorized users. To serve a user who wishes to check the condition of the railway tunnel in real-time, the monitoring data is transferred from the cloud database to the web. When the displacement at a measuring point exceeds a pre-set threshold, alarm is triggered and the corresponding information about the time of occurrence, position and deformation type is sent immediately to the railway managers. Considering that a suspension of train service due to false alarming is highly unexpected and that any missed or late alarm would risk more catastrophic consequences, the warning criteria must be carefully defined with advanced analysis tools to accurately and reliably pick out the time-variant deformation profiles and recognize all critical deformations after eliminating the

abnormal responses due to man-made interferences or malfunctioning of FBG bending gauges, which is why a workstation is required for data processing in time. The algorithms incorporated in the warning system will be detailed in other papers related to this study.

3. Experimental verification

3.1 Apparatus and test set-up

To verify the capability and feasibility of the devised railway tunnel deformation monitoring system using FBG bending gauges, a test platform is built up at The Hong Kong Polytechnic University for the purpose of experimental verification. As shown in Fig. 9, the platform is built to simulate different patterns of deformation in railway tunnels: five 500 mm×500 mm×500 mm concrete blocks are fixed on the ground in a 3000 mm distance to represent rail slabs. An electronic linear module is attached at each concrete block for generating transverse movements in a range of ±25 mm to simulate the displacement of the railway tunnel.
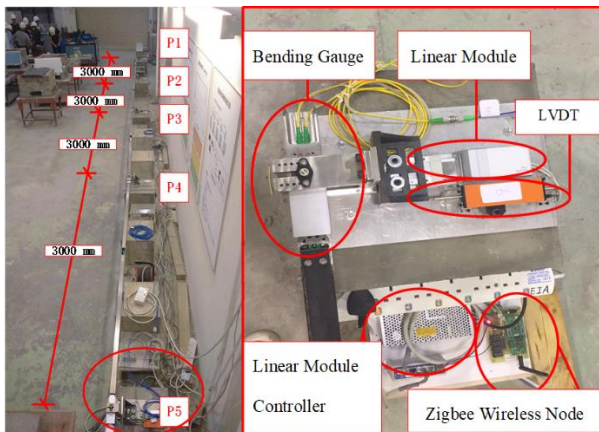

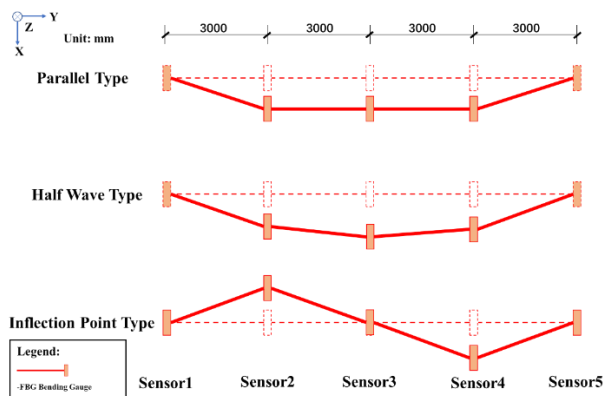Fig. 9 Built-up test platform for experimental verification

Fig. 10 Three deformation patterns tested in experiments

The electronic linear modules receive commands from the control panel through ZigBee wireless nodes to actuate displacement. Five FBG bending gauges interconnected by 3000 mm long rigid rods are deployed on the concrete blocks for displacement measurement. Five linear variable differential transformers (LVDTs) with a measurement range of ±25 mm and a resolution of 0.05 mm are installed as a reference to verify the measurement accuracy of the FBG bending gauge system.

3.2 Tunnel deformation simulation tests

In consideration of possible deformation situations in real railway tunnels, three patterns of deformation were tested in the verification experiments. As illustrated in Fig. 10, with the measuring point at sensor 1 being fixed and small displacement being imposed at sensor 5 to accommodate different situations, the deformation patterns are classified into three categories: parallel pattern, half-wave pattern and inflection-point pattern, respectively, in accordance with the corresponding geometric shapes.

During the experiments, commands were sent to the electronic linear modules through the ZigBee wireless nodes to initiate displacements, which were measured by the LVDTs and the FBG bending gauge system respectively. For each deformation pattern, a series of step-forward increasing displacements were tested. Figs. 11 to 13 show a comparison of the measurement results by the LVDTs and by the FBG bending gauge system for the three patterns under different displacement levels. It is seen from the figures that all the three deformation patterns are well captured by both the LVDTs and the FBG bending gauge system from small to large displacement amplitudes, and there is no significant difference between the measurement results obtained by the two sensing systems.

To further quantify the difference, the measured displacements by the two systems and the absolute errors by taking the LVDT results as a reference are tabulated in Tables 1 to 3. It is seen from the tables that the absolute errors between the measurement results from the FBG bending gauge system and the LVDTs are basically within ±1 mm with an absolute average level of 0.5 mm. The absolute errors are not affected by the amplitude of displacement being measured; while the relative errors of the measurement results are large when the displacement is 3mm or smaller, but the relative error is generally less than 10% when the displacement goes beyond 5 mm. The errors are thought to be mainly from loosening at the connection point between the bending gauge and the rigid rod, which leads to an extra angle of rotation. For railway tunnels, the critical deformation threshold for alarming is usually set to be 10 mm and the absolute error should not be larger than ±2 mm with every 10 meters of length measured. The total length of the test platform in this study is 12 m. From the experimental results, the FBG bending gauge system is proven to satisfy the required accuracy in the monitoring of different patterns of tunnel deformation.
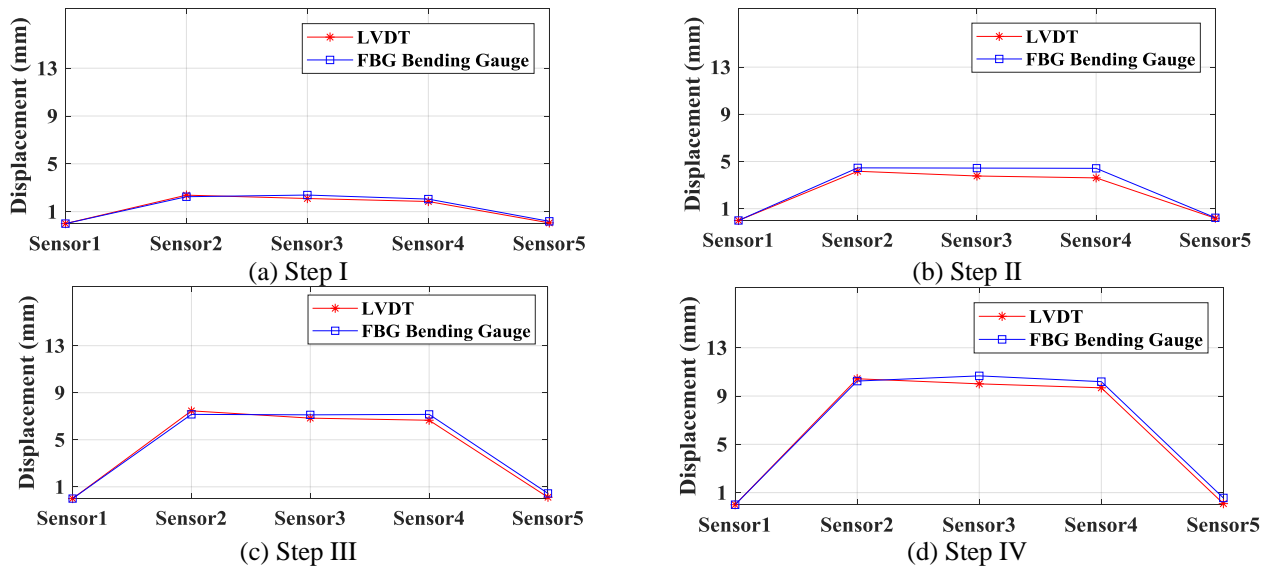
Fig. 11 Measurements by LVDT and devised monitoring system for parallel pattern
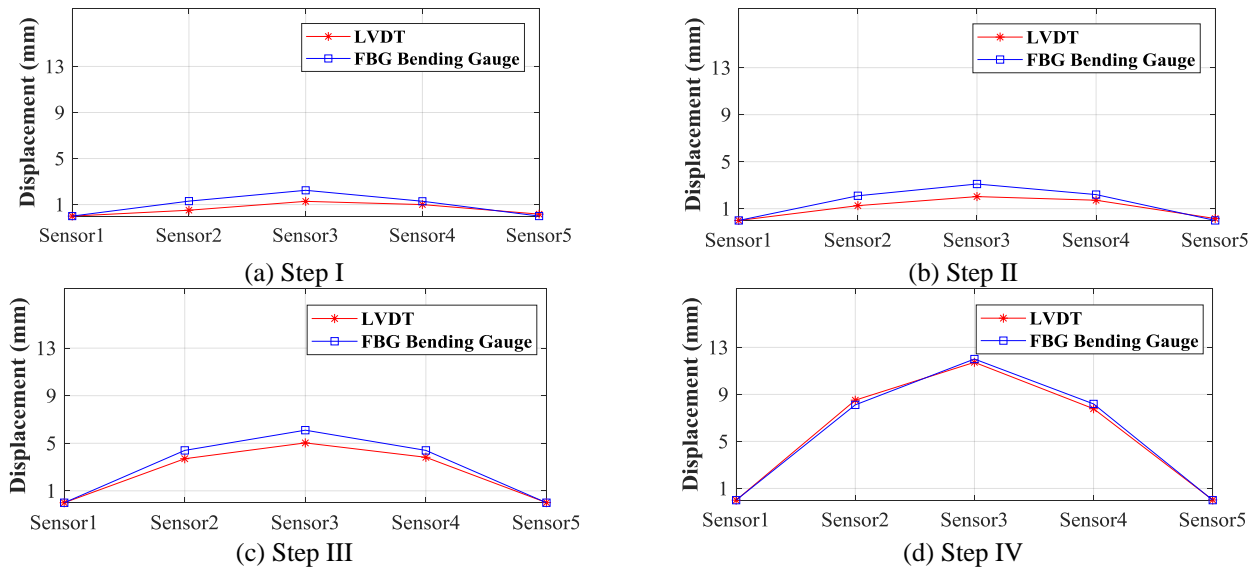

Fig. 12 Measurements by LVDT and devised monitoring system for half-wave pattern

Table 1 Comparison between LVDT and devised monitoring system for parallel pattern (Unit: mm)

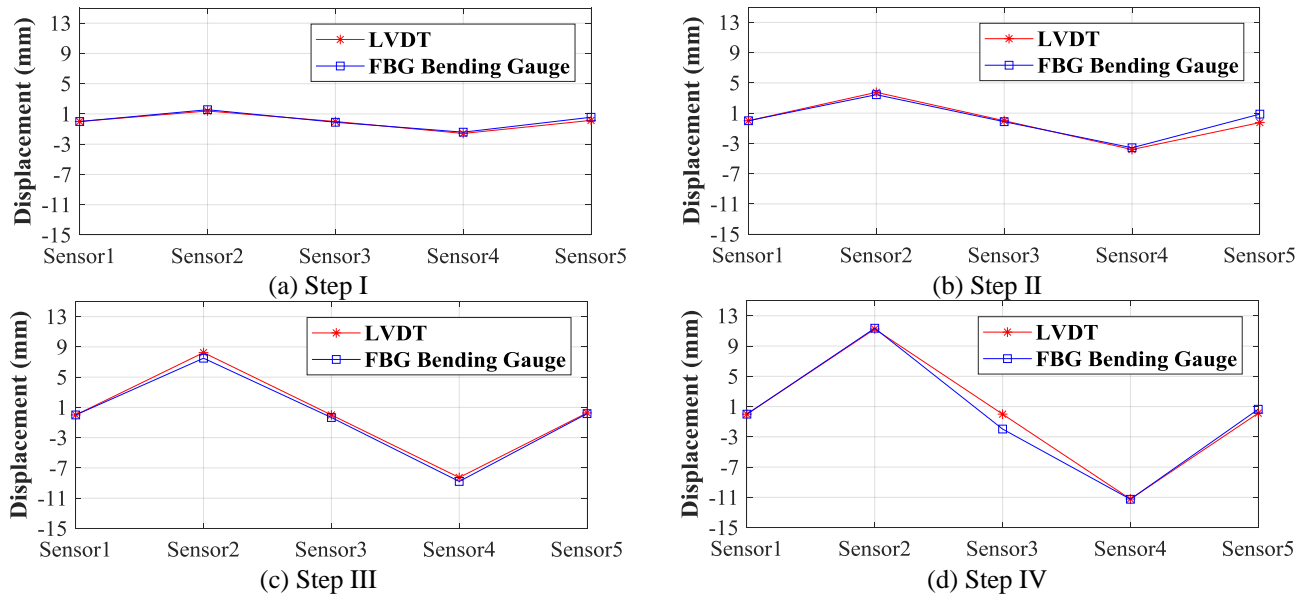|	Sensor 2			Sensor 3			Sensor 4			Sensor 5		
	LVDT	FBG Bending Gauge	Absolute error	LVDT	FBG Bending Gauge	Absolute error	LVDT	FBG Bending Gauge	Absolute error	LVDT	FBG Bending Gauge	Absolute error
WC 1	2.38	2.25	0.13	2.1	2.39	-0.29	1.85	2.05	-0.2	0.06	0.19	-0.13
WC 2	4.17	4.46	-0.29	3.77	4.44	-0.67	3.61	4.42	-0.81	0.19	0.23	-0.04
WC 3	7.46	7.16	0.3	6.84	7.12	-0.28	6.66	7.16	-0.5	0.11	0.44	-0.33
WC 4	10.43	10.24	0.19	10.01	10.67	-0.66	9.68	10.19	-0.51	0.09	0.56	-0.47

Fig. 13 Measurements by LVDT and devised monitoring system for inflection-point pattern

Table 2 Comparison between LVDT and devised monitoring system for half-wave pattern (Unit: mm)

	Sensor 2			Sensor 3			Sensor 4			Sensor 5		
	LVDT	FBG Bending Gauge	Absolute error	LVDT	FBG Bending Gauge	Absolute error	LVDT	FBG Bending Gauge	Absolute error	LVDT	FBG Bending Gauge	Absolute error
WC 1	0.51	1.3	0.79	1.28	2.24	0.96	1	1.29	0.29	0.17	1.29	0.12
WC 2	1.26	2.1	0.84	2.03	3.1	1.07	1.72	2.2	0.48	0.16	2.2	0.04
WC 3	3.7	4.4	0.7	5.03	6.1	1.07	3.82	4.4	0.58	0.01	4.4	-0.14
WC 4	8.51	8.11	-0.4	11.73	12.01	0.28	7.78	8.19	0.41	0.02	8.19	-0.26

Table 3 Comparison between LVDT and devised monitoring system for inflection-point pattern (Unit: mm)

	Sensor 2			Sensor 3			Sensor 4			Sensor 5		
	LVDT	FBG Bending Gauge	Absolute error	LVDT	FBG Bending Gauge	Absolute error	LVDT	FBG Bending Gauge	Absolute error	LVDT	FBG Bending Gauge	Absolute error
WC 1	1.39	1.56	-0.17	0	-0.1	0.1	-1.58	-1.41	-0.17	0.15	0.56	-0.41
WC 2	3.75	3.44	0.31	0	-0.13	0.13	-3.81	-3.58	-0.23	-0.25	0.87	-1.12
WC 3	8.24	7.5	0.74	0	-0.34	0.34	-8.27	-8.79	0.52	0.27	0.17	0.1
WC 4	11.25	11.36	-0.11	0	-1.97	1.97	-11.22	-11.25	0.03	0.13	0.65	-0.52

4. Real-time monitoring of in-service HSR tunnel

4.1 On-site implementation

After experimentally verifying the capability of the FBG bending gauges in laboratory, the devised railway tunnel deformation monitoring system was implemented on an in-service HSR tunnel. A total of 28 bending gauges were installed on one side of the rail slab to cover a length of 81 m in the longitudinal direction, with rigid rods of 3000 mm long each connecting two adjacent FBG bending gauges. A hinged support is designed for installation of each FBG

bending gauge on the rail slab (Fig. 14).

Unlike the conditions in conventional highway tunnels or laboratory environment, forced vibrations of the tunnel structure caused by passing trains should be considered as a potential influential factor to real-time monitoring of railway tunnels, especially in the orientation of measurement. It should be assured that the whole set of measuring mechanism does not suffer from resonance which would greatly increase the error in measurements. For this reason, the natural frequencies of the hinged support and the connecting rod were measured by carrying out a hammer impact test after their implementation to the
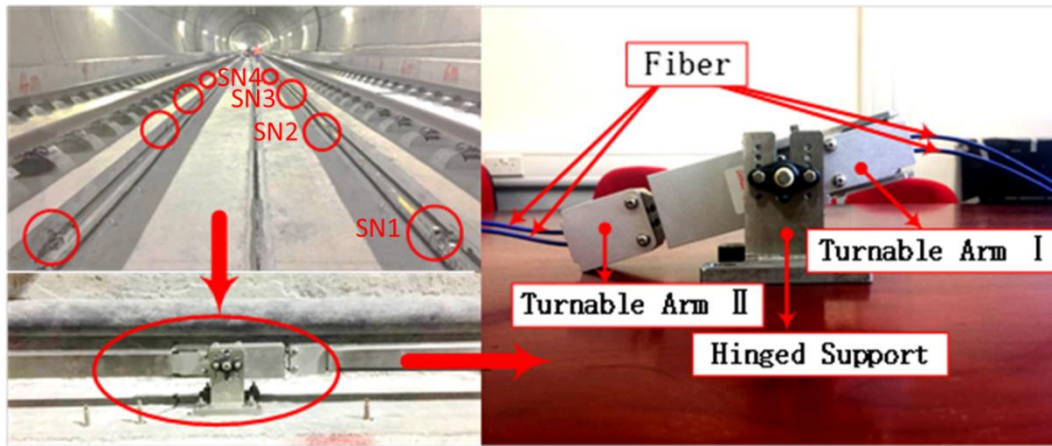
Fig. 14 Implementation of devised monitoring system in an in-service HSR tunnel
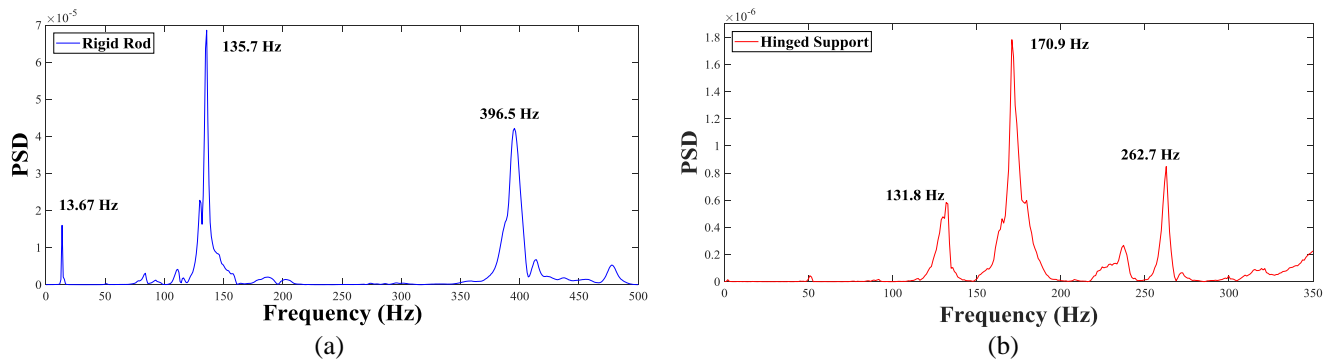

(a)

(b)

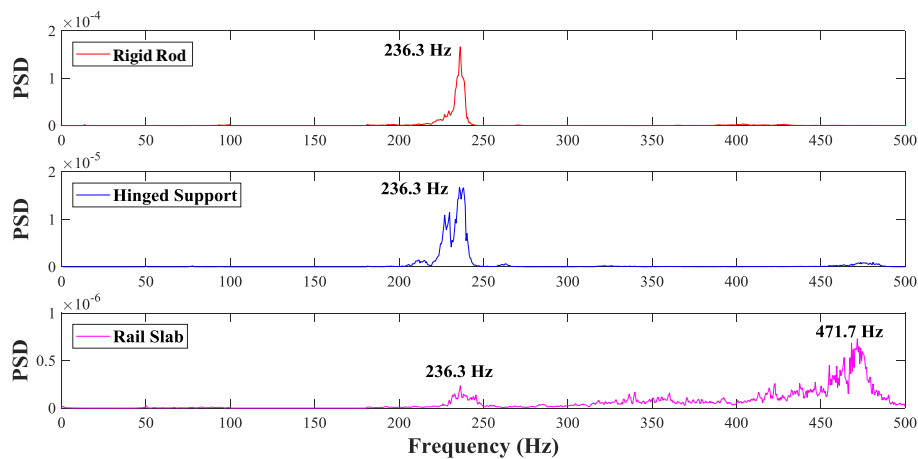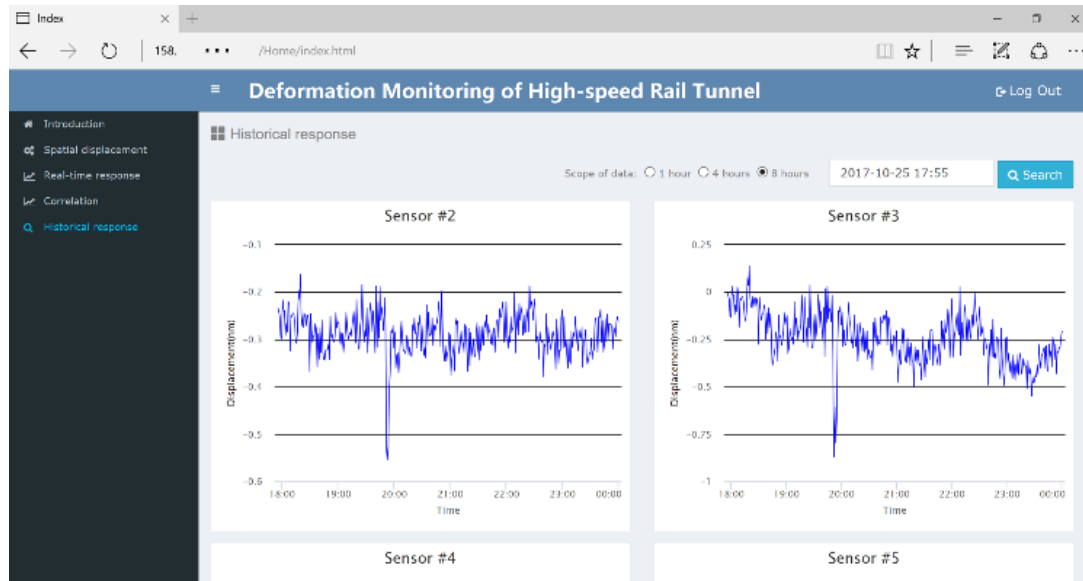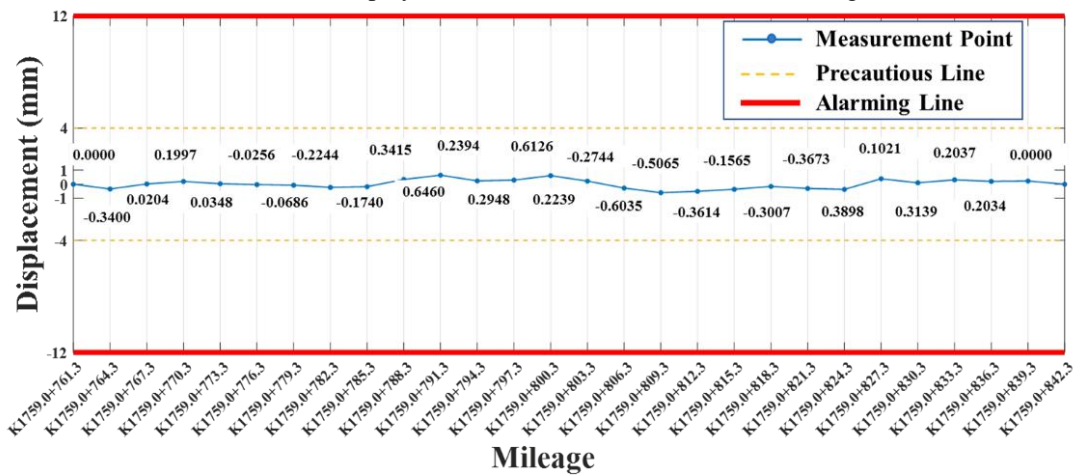Fig. 15 Natural frequencies of (a) rigid rod and (b) hinged support

Fig. 16 PSDs of rigid rod, hinged support and rail slab during the passage of a train

HSR tunnel. The implemented sensors are numbered as SN1 to SN 28. The hinged support of the bending gauge deployed at point SN3 and the rigid rod between point SN2 and point SN3, as shown in Fig. 14, were chosen for the hammer testing. The natural frequencies of the two parts were determined, and the power spectral densities (PSD) were plotted in Fig. 15, respectively.

The natural frequencies for the first three modes of the hinged support are 131.8 Hz, 170.9 Hz and 262.7 Hz, while those for the rigid rod are 13.67 Hz, 135.7 Hz, 395.5 Hz. After in-situ installation of the 28 FBG bending gauges, the forced frequencies of the hinged support, rigid rod and rail slab were measured again during the passage of a high-speed train. The PSDs of the three components are plotted

(a) Website for display and visualization of real-time monitoring data

(b) Real-time profile obtained by an array of 28-node FBG bending gauges

Fig. 17 Real-time web-based visualization of monitoring data from a HSR tunnel

in Fig. 16. The forced frequencies caused by the passing train are 236.3 Hz for the rigid rod, 236.3 Hz for the hinged support, and 236.3 Hz and 471.7 Hz for the rail slab. It can be concluded that passing trains will not cause resonance of the measuring mechanism.

4.2 Real-time web-based visualization and alarming

As mentioned in Sub-section 2.4, the real-time monitoring data are uploaded onto a cloud database for storage through cellular network. For all 28 bending gauges, the sampling rate is 1 datum per minute, which is sufficient for railway tunnel deformation monitoring since the deformation is a slow-varying process. Also, the low sampling rate is suitable since the cellular network in a railway tunnel is usually inadequate for broadband data transmission. A front-end website has been developed using Python and JavaScript for real-time data display and visualization. The displacements measured from all 28 bending gauges are updated every minute and can be

viewed directly online as illustrated in Fig. 17(a); and Fig. 17(b) shows the real-time profile obtained by the 28-node FBG bending gauge chain which is also updated every minute. In Fig. 17(b), each bending gauge is labelled by its corresponding location of installation in the HSR tunnel as mileage marked on the rail slab.

It should be noted that some outlier data were seen in Fig. 17(a). This phenomenon is common and mainly due to the reasons that the FBG interrogators used in the field are different from those used in lab experiments with a higher sampling frequency, which makes them more vulnerable to environmental interferences, and that the interrogators are exposed under a harsher environment in operating railway tunnel. The fluctuations due to the above reasons are within an acceptable level of ±1 mm and are automatically eliminated in the data processing procedure. It is also worth mentioning that sensor 2 and sensor 3 exhibit a similar pattern of abnormal points because these two sensors share the same FBG interrogator, which would affect all the sensors it is in charge of at the same time upon any

interference.

As illustrated in Fig. 17(b), all 28 FBG bending gauges implemented in the HSR tunnel are in normal operation, and the measurement values are around the zero line with fluctuations no more than ±1 mm. The fluctuations mainly come from trivial vibrations of the measuring mechanism due to environmental factors such as winds and passing trains, and can be easily filtered out in outlier detection algorithm. Manual inspections are planned in the tunnel to further validate the effectiveness and reliability of the monitoring system. Displacement of ±4 mm are set as the precautious lines, and railway operators and managers will be notified immediately to be ready to take measures when either precautious line is reached or exceeded. When either threshold of ±12 mm is reached, warning is alarmed at once to inform the authority to make decisions and take actions immediately.

5. Conclusions

In this study, a novel online railway tunnel deformation monitoring system using FBG sensing technology has been developed, tested, and implemented in-situ. FBG bending gauges with temperature self-compensation capacity have been devised specifically for the railway tunnel monitoring task. After validating the capability to compensate the influence caused by temperature variation, verification experiments using LVDTs as reference sensors have been carried out which demonstrate that the FBG bending gauge system satisfies the required accuracy of measuring different patterns of tunnel deformation. In-situ implementation of 28 FBG bending gauges on an in-service HSR tunnel has been accomplished. The whole system shows a good performance in anti-interference to passing trains, and stable monitoring data are being continuously collected. The data are stored, processed and analyzed in a workstation, and displayed for real-time visualization via a front-end website. Early warning is expected to be alarmed upon exceedance of the measured tunnel deformation over a certain threshold. In the next step, the monitoring system will be expanded to deploy more FBG bending gauges along the longitudinal direction to cover the full length of the tunnel, and to deploy more arrays at different cross-sectional positions of the tunnel to attain a full spatial-temporal profile of the tunnel deformation.

Acknowledgements

References

Bernardo-Sánchez, A. and Arlandi-Rodríguez, M. (2014), "Procedure for obtaining and analyzing the diametric deformation of a tunnel by means of tape extensometer convergence measures", *Proceedings of the ISRM Regional Symposium-EUROCK 2014,* International Society for Rock Mechanics and Rock Engineering, Spain.

Chan, T.H.T., Yu, L., Tam, H.Y., Ni, Y.Q., Liu, S.Y., Chung, W.H. and Cheng, L.K. (2006), "Fiber Bragg grating sensors for structural health monitoring of Tsing Ma Bridge: background and experimental observation", *Eng. Struct.*, **28**(5), 648-659.

Ding, L.Y., Zhou, C., Deng, Q.X., Luo, H.B., Ye, X.W., Ni, Y.Q. and Guo, P. (2013), "Real-time safety early warning system for cross passage construction in Yangtze riverbed metro tunnel based on the internet of things", *Automat. Constr.*, **36**, 25-37.

Ho, Y.T., Huang, A.B. and Lee, J.T. (2006), "Development of a fibre Bragg grating sensored ground movement monitoring system", *Meas. Sci. Technol.*, **17**(7), 1733.

Kavvadas, M.J. (2005), "Monitoring ground deformation in tunnelling: current practice in transportation tunnels", *Eng. Geol*, **79**(1), 93-113.

Kontogianni, V., and Stiros, S. (2003), "Tunnel monitoring during the excavation phase: 3-D kinematic analysis based on geodetic data", *Proceedings of the 11th FIG Symposium on Deformation Measurements*, Santorini.

Luo, Y., Chen, J., Xi, W., Zhao, P., Qiao, X., Deng, X. and Liu, Q. (2016), "Analysis of tunnel displacement accuracy with total station", *Measurement*, **83**, 29-37.

Metje, N., Chapman, D.N., Rogers, C.D.F., Henderson, P. and Beth, M. (2008), "An optical fiber sensor system for remote displacement monitoring of structures -- prototype tests in the laboratory", *Struct. Health Monit.*, **7**(1), 51-63.

Ni, Y.Q., Xia, Y., Liao, W.Y. and Ko, J.M. (2009), "Technology innovation in developing the structural health monitoring system for Guangzhou New TV Tower", *Struct. Control Health Monit.*, **16**(1), 73-98.

Ordóñez, C., Argüelles, R., Sanz-Ablanedo, E. and Roca-Pardiñas, J. (2016), "Deformation analysis in tunnels through curve clustering", *Appl. Math. Model.*, **40**(2), 1325-1332.

Pei, H.F., Teng, J., Yin, J.H. and Chen, R. (2014), "A review of previous studies on the applications of optical fiber sensors in geotechnical health monitoring", *Measurement*, **58**(3), 207-214.

Pejić, M. (2013), "Design and optimisation of laser scanning for tunnels geometry inspection", *Tunnel. Underground Space Technology*, **37**, 199-206.

Scaioni, M., Barazzetti, L., Giussani, A., Previtali, M., Roncoroni, F. and Alba, M.I. (2014), "Photogrammetric techniques for monitoring tunnel deformation", *Earth Sci. Inform.*, **7**(2), 83-95.

Tse, C. and Luk, J. (2011), "Design and implementation of automatic deformation monitoring system for the construction of railway tunnel: A case study in West Island Line", *Joint International Symposium on Deformation Monitoring*, Hong Kong.

Wright, P. (2010), "Assessment of London underground tube tunnels - investigation, monitoring and analysis", *Smart. Struct. Syst.*, **6**(3), 239-262.

Ye, X.W., Ni, Y.Q. and Yin, J.H. (2013), "Safety monitoring of railway tunnel construction using FBG sensing technology", *Adv. Struct. Eng.*, **16**(8), 1401-1409.

Ye, X.W., Su, Y.H. and Han, J.P. (2014), "Structural health monitoring of civil infrastructure using optical fiber sensing technology: A comprehensive review", *Sci. World J.*, **2014**(1), 11 pages.

Yoon, J.S., Sagong, M., Lee, J.S. and Lee, K.S. (2009), "Feature extraction of a concrete tunnel liner from 3D laser scanning data", *NDT E Int.*, **42**(2), 97-105.

Yoshida, Y., Kashiwai, Y., Murakami, E., Ishida, S. and Hashiguchi, N. (2002), "Development of the monitoring system for slope deformations with fiber Bragg grating arrays", *Proceedings of the SPIE's 9th Annual International Symposium on Smart Structures and Materials*, San Diego, California.

Zhu, H.H., Ho, A.N.L., Yin, J.H., Sun, H.W., Pei, H.F. and Hong, C.Y. (2012), "An optical fibre monitoring system for evaluating the performance of a soil nailed slope", *Smart. Struct. Syst.*, **9**(5), 393-410.